



# Tracking the progress of inflammation with PET/MRI in a canine model of myocardial infarction

B. Wilk,<sup>a,b,d</sup> H. Smailovic, BSc,<sup>a,c</sup> G. Wisenberg, MD,<sup>a,e</sup> J. Sykes,<sup>a</sup> J. Butler,<sup>a</sup>  
M. Kovacs, PhD,<sup>a,b,c</sup> J. D. Thiessen, PhD,<sup>a,b,c,d</sup> and F. S. Prato, PhD<sup>a,b,c,d</sup>

<sup>a</sup> Lawson Health Research Institute, London, Canada

<sup>b</sup> Department of Medical Biophysics, Western University, London, Canada

<sup>c</sup> Department of Medical Imaging, Western University, London, Canada

<sup>d</sup> Collaborative Graduate Program in Molecular Imaging, Western University, London, Canada

<sup>e</sup> MyHealth Centre, Arva, Canada

Received Jul 22, 2020; accepted Nov 28, 2020

doi:10.1007/s12350-020-02487-5

**Background.** Following myocardial infarction, tissue undergoes pathophysiological changes involving inflammation and scar tissue formation. However, little is known about the pathophysiology and prognostic significance of any corresponding changes in remote myocardium. The aim of this study was to investigate the potential application of a combined constant infusion of <sup>18</sup>F-FDG and Gd-DTPA to quantitate inflammation and extracellular volume (ECV) from 3 to 40 days after myocardial infarction.

**Methods.** Eight canine subjects were imaged at multiple time points following induction of an MI with a 60-minute concurrent constant infusion of Gd-DTPA and <sup>18</sup>F-FDG using a hybrid PET/MRI scanner.

**Results.** There was a significant increase in ECV in remote myocardium on day 14 post-MI ( $P = .034$ ) and day 21 ( $P = .021$ ) compared to the baseline. ECV was significantly elevated in the infarcted myocardium compared to remote myocardium at all time points post-MI (days 3, 7, 14, 21, and 40) ( $P < .001$ ) while glucose uptake was also increased within the infarct on days 3, 7, 14, and 21 but not 40.

**Conclusions.** The significant increase in ECV in remote tissue may be due to an ongoing inflammatory process in the early weeks post-infarct. (J Nucl Cardiol 2022;29:1315–25.)

**Key Words:** Inflammation • Myocardial ischemia and infarction • Microvascular dysfunction • MRI • PET • Hybrid imaging

## Abbreviations

IOT	Infarcted obstructed tissue
INOT	Infarcted not obstructed tissue
RT	Remote tissue
MI	Myocardial infarction
GBCA	Gadolinium-based contrast agent

FDG	<sup>18</sup> F-Fluorodeoxyglucose
ECV	Extracellular volume
EF	Ejection fraction
ESV	End-systolic volume
EDV	End-diastolic volume

**Supplementary information** The online version of this article (<https://doi.org/10.1007/s12350-020-02487-5>) contains supplementary material, which is available to authorized users.

The authors of this article have provided a PowerPoint file, available for download at SpringerLink, which summarizes the contents of the paper and is free for re-use at meetings and presentations. Search for the article DOI on SpringerLink.com.

The authors have also provided an audio summary of the article, which is available to download as ESM, or to listen to via the JNC/ASNC Podcast.

B. Wilk and H. Smailovic have contributed equally to this work.

Reprint requests: B. Wilk, Lawson Health Research Institute, London, Canada; [bwilk@uwo.ca](mailto:bwilk@uwo.ca)

1071-3581/\$34.00

Copyright © 2021 American Society of Nuclear Cardiology.

---

**See related editorial, pp. 1326–1328**

---

## INTRODUCTION

After a myocardial infarction (MI), patients remain at risk of adverse events, including heart failure.<sup>1</sup> Risk factors for these adverse events include infarct size<sup>2,3</sup> and extent of microvascular obstruction.<sup>4</sup> Both are independent predictors of left ventricular remodeling. Inflammation also plays a key role in the response to infarction, and its evolution will play a key role in determining how the left ventricle remodels. Both MRI and FDG-PET may provide insights into the evolution of myocardial injury and inflammation.

Using MRI, T1 maps can be obtained and used to measure the extracellular volume, an indicator of tissue edema, a common accompaniment of inflammation. ECV is elevated within infarcted tissue post-MI, starting in the first few hours.<sup>5</sup> However, little is known about the ECV in remote non-infarcted, non-ischemic myocardium as the left ventricle remodels.<sup>6</sup> In such tissue, fibrosis, cellular inflammation, and edema may evolve gradually which would result in a slow increase in ECV, which might only be measurable over extended periods of time (months).<sup>7,8</sup>

In addition to defining the extent of irreversible injury, the delayed enhancement protocol also provides a volume measure of microvascular obstruction within the infarct which we designate hereafter as infarcted obstructed tissue or IOT. IOT has very compromised blood flow with reduced tracer delivery. As a result, little is known about the ECV in the IOT and how it changes in time post-MI.

In order to quantitate ECV in remote tissue (RT), infarcted tissue excluding any region with significant microvascular obstruction, infarcted non-obstructed tissue or INOT, and IOT, single-slice breath hold T1 maps need to be acquired spanning the entire heart.<sup>9–11</sup> However, this requires acquisition during which the concentration of GBCA in the blood and tissue should not be changing significantly, as it normally would following a bolus injection.<sup>9–11</sup> However, it has been known for some time that a bolus injection followed by a constant infusion of GBCA, given the correct timing and dose distribution between the bolus and constant infusion, achieves relatively rapid constant blood concentrations.<sup>9–12</sup> Despite this, few studies have investigated just using a prolonged constant infusion to measure ECV in the RT, INOT, and IOT.<sup>13</sup>

Post-MI cellularly mediated inflammatory processes clear out myocardial cellular debris and stabilize the region of infarction with scar tissue. When using FDG to image macrophage-mediated cardiac inflammation, an important consideration is effective suppression of the

glucose uptake by cardiomyocytes to get an accurate picture of inflammation, without the confounding effect of myocardial glucose uptake. This is generally achieved with one or more of: fasting, a high-fat diet, heparin injection, and in animals, a lipid infusion.<sup>14</sup> In addition to the concern regarding suppression of myocardial glucose uptake, an additional concern with FDG-PET imaging in acute MI is the potential effect of IOT on the apparent inflammation profile: lower FDG activity in the center of the infarct (i.e., the IOT) may be primarily the result of reduced delivery of this tracer as a result of the severely compromised flow. Since myocardial infarction patients with IOT have poorer outcomes, it is imperative to be able to accurately quantitate the inflammatory processes within this region (without the confounding effects of compromised tracer delivery), in order to plan future interventions to improve prognosis. Previously, a constant infusion has been used in the brain to penetrate the ischemic region post-stroke.<sup>15</sup> We propose that a constant infusion of Gd-DTPA and FDG would allow penetration of the IOT to allow better characterization of the inflammatory response, both macrophage mediated, and that associated with tissue fibrosis and edema, without the constraints of compromised tracer delivery.

Here, we have investigated the potential application of a simple combined constant infusion of Gd-DTPA and FDG to quantitate inflammation, ECV and function in RT, INOT, and IOT in a canine model of permanent coronary artery occlusion from 3 to 42 days post-MI.

## METHODS

### Animals and Surgical Preparation

This study was approved by the Animal Care Committee of Western University. Eight adult, female, bred-for-research hounds were used. Anesthesia for surgery and imaging was induced using propofol and maintained with 1.5% to 2% isoflurane. Animals underwent imaging at baseline (n = 5), 3–4 (n = 6), 7 to 8 (n = 7), 14 to 15 (n = 6), 21 to 22 (n = 8), and 38 to 44 (n = 8) days post-MI (Figure 1). Due to technical difficulties, not all animals were imaged at all time points. MI was induced by permanently placing a snare ligature around the left anterior descending coronary artery during left thoracotomy.

### PET Imaging

Animals were fasted between 16 and 21 hours before the start of imaging. To further suppress myocardial glucose uptake, twenty minutes before the constant infusion of FDG, 2000 units of heparin were administered intravenously, and an infusion of 20% lipid (Intralipid; Baxter Healthcare Corporation) at a rate of 0.25 mL/min/kg was administered intravenously over a 50-minute period starting immediately after the administration of heparin (see figure S3 for a sample image). Note that whereas, in humans, diet and heparin are

sufficient for 95% suppression,<sup>14</sup> in canines, intralipid infusion is also needed as we have previously reported.<sup>16</sup>

A 60-minute constant infusion of both FDG (0.17 MBq/min/kg; fludeoxyglucose (<sup>18</sup>F) injection, produced in-house at the Lawson Cyclotron Facility) and Gd-DTPA (0.004 mmol/min/kg for a total dose of 0.24 mmol/kg, Magnevist; Bayer Inc.) was started simultaneously with the beginning of the list-mode PET acquisition. In addition to the 60-minute infusion, the PET acquisition was extended to a further 10-minute washout in 3 dogs and a 30-minute washout in 5 dogs. The PET data were reconstructed in 3-minute frames using a 3D ordered-subset expectation maximization reconstruction (3 iterations, 21 subsets, 172 × 172 × 127 matrix size, zoom of 2 and 4 mm Gaussian filter). MR-based attenuation correction was achieved using a two-point Dixon MRI sequence and segmented into water, fat, lung, and air with constant attenuation coefficients for each tissue.<sup>17</sup> The PET voxel size was 2.09 × 2.09 × 2.03 mm.

### Cardiac MR Imaging

MR imaging was started 60 minutes prior to beginning of the constant infusion. Sequences included short-axis cine stacks of the left ventricle synchronized to the ECG signal (true fast imaging with steady-state free precession (True-FISP), slice thickness 6 mm, 256 × 216 voxels, voxel size 1.09 × 1.09 mm, ~ 12 second acquisition time, based on heart rate) where each slice was acquired during a breath hold; a 3D T1-weighted image (ECG-triggered inversion recovery sequence with navigator echo for respiratory gating, 256 × 200 × 112 voxels, voxel size 0.625 × 0.625 × 0.9 mm, ~ 4 minute

acquisition time, based on heart and respiratory rate); T1 maps (ECG-triggered modified look-locker inversion recovery sequence, slice thickness 6 mm, 256 × 144 voxels, voxel size 1.09 × 1.09 mm, ~ 12 second acquisition time, based on heart rate) in a single breath hold to acquire 2-chamber and 4-chamber views of the heart (Siemens Work In Progress). In 7 animals, T1 maps and 3D T1-weighted images were acquired in 10 minute intervals. In the other animal, 4-chamber view T1 maps were acquired every 3 minutes and a 3D T1-weighted image was acquired 70 minutes into the PET scan (i.e., 10 minutes after the infusion was stopped). See Figure 1 for details on the timing of both the MRI and PET data acquisitions.

### Data Analysis

**Regions of interest** Regions of interest (ROIs) were manually drawn onto the final Gd-enhanced T1 map which was then automatically transferred to all other T1 maps. The ROIs outlined were the IOT, the INOT, two samples of RT, and the blood pool. Note that the IOT only included tissue with microvascular obstruction, and the INOT was all other infarcted tissue, excluding the IOT. The 2D ROIs were then also transferred to the corresponding slice of PET data. Figure 2 shows the selection of the three regions of interest (RT, INOT, and IOT) and the selection of the blood pool region within the left ventricular cavity all taken 10 minutes after the 60-minute constant infusion. Manual adjustment of some images in the series was applied to offset changes in heart position. Edges were also avoided when drawing ROIs to

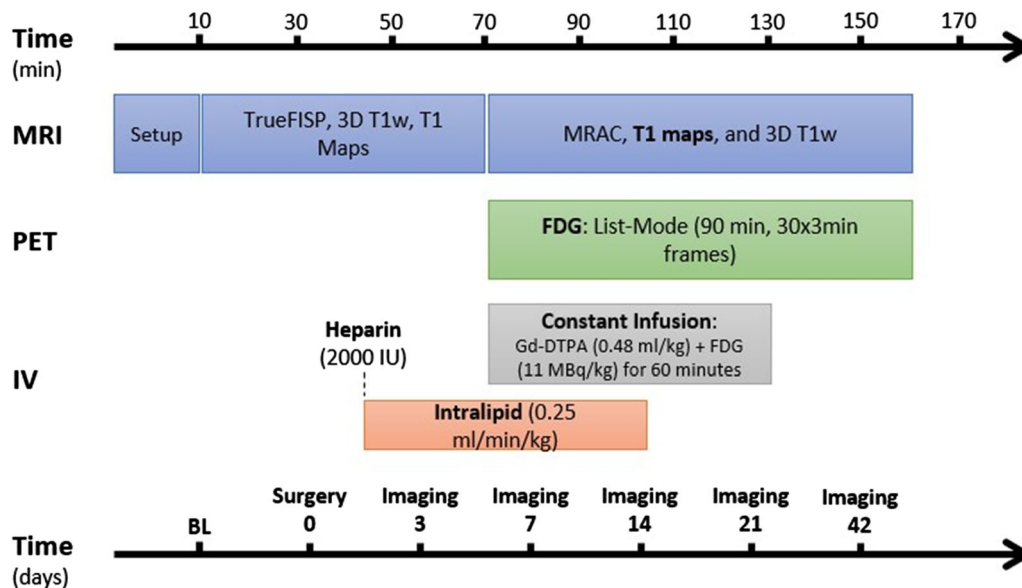


**Figure 1.** Experimental Protocol: After the subject was setup in the MR scanner, MRAC, localizers, pre-contrast images, and cine images were acquired. During this time, heparin was injected and lipids were infused. Then, a constant infusion of Gd-DTPA and FDG was started, and T1 maps and 3D T1-weighted images were acquired in conjunction with FDG list-mode data.

minimize partial volume averaging from voxels at the myocardial-blood pool border.

**Glucose metabolism** FDG concentration curves of all ROIs were fit to the Patlak model<sup>18</sup> using the following equation:

$$[FDG(t)]_i = K_i \int_0^t [FDG(\tau)]_p d\tau + (v_e^p + v_p^p) [FDG(t)]_p,$$

where  $[FDG(t)]_i$  is the concentration of FDG in tissue  $i$ , including corrections outlined below,  $K_i$  the influx constant is proportional to the rate of glucose metabolism in tissue  $i$ , and  $[FDG(t)]_p$  is the arterial plasma concentration input function, defined as the blood pool ROI in the left ventricular cavity corrected for the hematocrit (assumed to be 0.45).<sup>19</sup>  $v_e^p$  is the equilibrium space of the extravascular exchangeable region and  $v_p^p$  the plasma space.

The influx constant,  $K_i$ , is the slope of the plot of  $\frac{[FDG(t)]_i}{[FDG(t)]_p}$  vs  $\frac{\int_0^t [FDG(\tau)]_p d\tau}{[FDG(t)]_p}$ , once the slope is constant, at 12 minutes after the start of the constant infusion.  $[FDG(t)]_b$  was corrected by the glucose plasma:whole blood ratio ( $P$ ) of 1.375<sup>20</sup> and the haematocrit (Hct), i.e.,  $[FDG(t)]_p = [FDG(t)]_b \cdot P / (1 - Hct)$ , where  $[FDG(t)]_b$  is the blood concentration. The tissue concentration was corrected for the spillover effect based on object size in PET using a recovery coefficient (RC) of 0.7 determined for the myocardial wall in our PET/MRI imaging system, i.e.,  $[FDG(t)]_i = [FDG(t)]_p / RC - (1 - RC) [FDG(t)]_b / RC$ ,<sup>21,22</sup> where  $[FDG(t)]_i$  is the uncorrected tissue concentration.

**Extracellular volume fraction** ECV maps calculated at the 60-minute time point in the constant infusion were used to compare changes over time. For the estimation of ECV, equilibrium was assumed to be reached when the difference in ECV between acquisitions was less than 5%, as done by White et al,<sup>23</sup> 76 out of 868 T1 maps could not be analyzed due to excess noise and were excluded. ECV was calculated using the formula:

$$ECV = (1 - hct) \times \frac{\frac{1}{\text{postcontrast} \tau_{1\text{myo}}} - \frac{1}{\text{native} \tau_{1\text{myo}}}}{\frac{1}{\text{postcontrast} \tau_{1\text{blood}}} - \frac{1}{\text{native} \tau_{1\text{blood}}}}$$

**Volumes of IOT and INOT** To determine the volume of the IOT and INOT, gadolinium-enhanced 3D T1-weighted images were segmented by a single observer using the 3D Slicer Segment Editor (<http://www.slicer.org>).<sup>24</sup> Thresholds were determined for IOT, INOT, and RT and drawn using the threshold paint function. This threshold approached insured that the INOT did not include IOT.

**MRI measurement of heart function** Using Slicer to analyze the ECG-triggered short-axis TrueFISP image series, the blood pool can be segmented. A single operator defined the blood pool throughout the series and determined the phases of the cardiac cycle with the highest and the lowest blood volume. These were defined as the end-diastolic volume

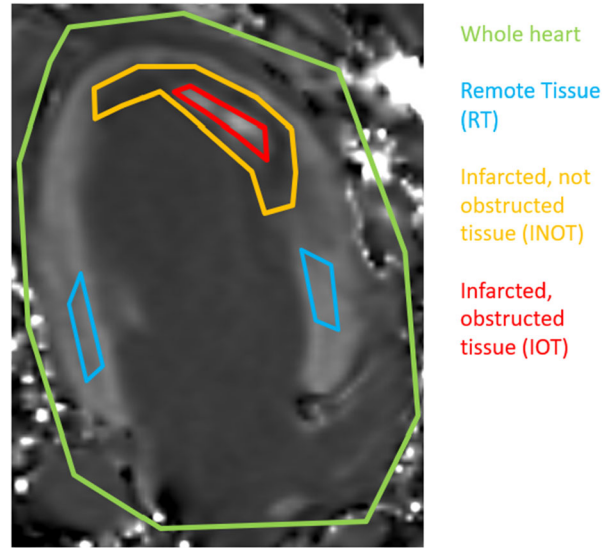


**Figure 2.** Glucose metabolism and extracellular volume (ECV) measurements were calculated at four separate regions (two in remote tissue (RT), one in infarcted not obstructed (INOT), excluding tissue with microvascular obstruction, and one in infarcted obstructed tissue (IOT)).

(EDV) and end-systolic volume (ESV). The ejection fraction (EF) was calculated using the equation:

$$EF = \frac{EDV - ESV}{EDV} \cdot 100\%.$$

These results were compared to the automatic segmentation generated with commercial cardiovascular image analysis software, circle cvi42 (Circle Cardiovascular Imaging Inc, Calgary), and were found to be within 5% when the same number of short-axis slices were used. As circle cvi42 failed in a number of sets of data, we report values from Slicer. Slices were excluded due to poor image quality, if the aorta was visible or if they were past the apex.

**Statistics** Statistical analysis was performed using GraphPad Prism (GraphPad Software, La Jolla, CA). All data are presented as mean  $\pm$  standard error of the mean. Repeated-measures analysis of variance (ANOVA) were performed on the days post-MI prior to washout and following washout. Comparison of differences in RT, INOT, and IOT as well as during washout of Gd-DTPA was assessed with paired and unpaired two-tailed  $t$  tests. A  $P$  value of  $< .05$  was considered to be statistically significant. Corrections for multiple comparisons were performed using a Bonferroni multiple comparison test.

## RESULTS

### Volume of IOT and INOT

Figure 3 shows the T1 maps determined every 10 minutes for one dog. Penetration over time into the IOT



can be seen. ROIs were drawn on the 70-minute map to allow for some washout from the blood pool. Measuring the volume of the INOT showed a decrease over time in all animals with a mean starting value of 15174 mm<sup>3</sup> at day 3 and a final value of 4939 mm<sup>3</sup> at day 43, as shown in Figure 4. Statistical differences were observed starting at day 14 ( $P = .014$ ) and then also on day 21 ( $P = .0031$ ) and day 43 ( $P = .0003$ ).

### Extracellular Volume

There was a significant increase in RT at minute 60 on day 14 ( $P = .0336$ ) and day 21 ( $P = 0.0205$ ) post-MI compared to the baseline healthy myocardial ECV as shown in figure 5. There was no significant difference in RT ECV on day 3 ( $P = .50$ ), day 7 ( $P = .086$ ), and at day 40 post-MI ( $P = .0597$ ) relative to the baseline myocardial ECV.

As shown in Figure 6, ECV was significantly elevated in the INOT myocardium at minute 60 compared to RT myocardium at all time points post-MI (days 3, 7, 14, 21, and 40) ( $P < .001$ ).

In the INOT at day 3, there was a significant increase at minute 60 compared to minute 50 ( $P = .024$ ). At all other days post-MI, there was no significant difference between minute 60 and minute 50 (day 7:  $P = .062$ ; day 14:  $P = .39$ ; day 21:  $P = .47$ ; day 40:  $P = .11$ ).

In the IOT, there was no significant difference in ECV at day 3 at minute 50 and minute 60 ( $P = .17$ ). There was a significant difference between minute 50 and 60 at day 7 ( $P < .01$ ); however, at all other time points, there were an insufficient number of canines with an IOT to do proper analysis ( $N = 3$  for day 14,  $N = 1$  for day 21,  $N = 0$  for 40 days).

Figure 7 shows ECV values for the INOT tissues for all canines post-MI as a function of 60-minute constant infusion followed by 30 minutes of washout. The measured ECV is significantly increased during the washout period of Gd-DTPA (see figure S1 in the supplemental data). This was also seen for the IOT tissue at day 3 at 70, 80, and 90 minute of washout and at day 7 at 90 minute while at days 14, 21, and 40, there were insufficient data for analysis as the IOT tended to resolve into INOT.

### Patlak Parameter Estimates

Figure 8 shows the Ki for all 8 animals in remote myocardium as a function of time post-MI. Although it appears that there was an increase in some animals early post-MI, no significant changes were seen (day 3:  $P = .38$ ; day 7  $P = .32$ ; day 14:  $P = .11$ ; day 21:  $P = 0.19$ ; day 43:  $P = .63$ ).

Figure 9 shows the glucose metabolism for the INOT, Ki, as a marker of glucose metabolism significantly exceeds baseline ( $0.00514 \pm 0.00045$ ) at all points other than day 43, when glucose metabolism returns to the baseline value. While day 3 is not significantly different from day 7, it is higher than all other values, showing that the inflammatory response appears largest within the first week of infarct. This decrease over time appears to be linear with an r value of 0.918 ( $P = .0278$ ).

The extravascular exchangeable volume in the INOT, calculated with the Patlak model, also undergoes significant changes post-MI, where days 7 ( $P = .0199$ ), 14 ( $P = .0015$ ), 21 ( $P = .0001$ ), and 42 ( $P < .0001$ ) are significantly higher than day 3 as shown in Figure S2.

Glucose metabolism in the IOT is increased at days 3 ( $P = .0332$ ) and 7 ( $P = .0042$ ) relative to baseline. There were not enough values for subsequent days to test significance, although in the remaining animals, it does appear to stay elevated.

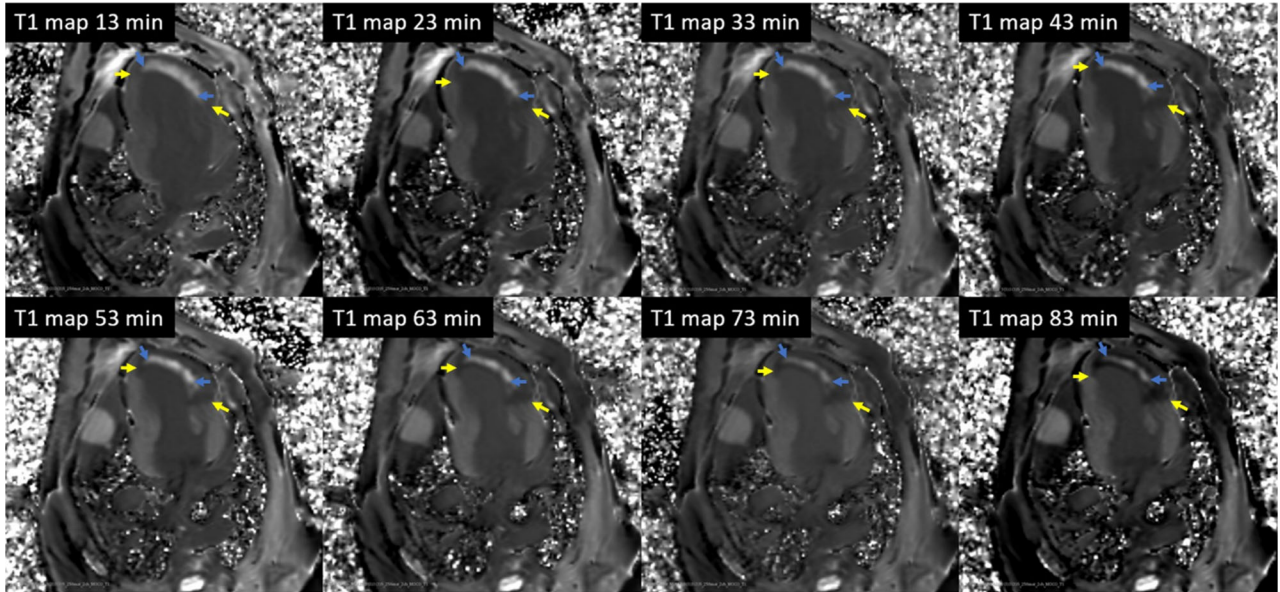
### Measurements of Cardiac Function

Figure 10 shows the ejection fraction (EF), end-diastolic volume (EDV), and end-systolic volume (ESV) for all animals. A sharp decrease in ejection fraction is visible at day 3 ( $P = .0013$ ) before it returns to a baseline value at day 7. The end-diastolic volume on the other hand does not show a difference while the ESV increases on day 3 ( $P = .0127$ ).

## DISCUSSION

In this study, we have applied PET/MR using a combined infusion of a gadolinium-based contrast agent and FDG to assess cell-based inflammation, myocardial fibrosis, and edema, in multiple regions of potential myocardial injury following an acute myocardial infarction. Accurate assessment of these processes can be compromised by issues of reduced tracer delivery, particularly within the central core of an infarction, where microvascular obstruction can markedly reduce blood flow. A single bolus injection of either tracer may not allow adequate penetration of these tracers into these areas of markedly compromised flow.

Although our group has previously demonstrated that concurrent constant infusions of Gd-DTPA and FDG can provide valid measures of ECV and <sup>18</sup>F-FDG in normal myocardium,<sup>13</sup> this is the first time that this injection strategy has been used to investigate RT, INOT, and IOT post-MI, and sequentially over several weeks. It is evident from Figure 5A that identical ECV values in RT can be measured after 20 to 30 minutes after the onset of a constant infusion until 30 minutes after terminating the constant infusion implying that the



**Figure 3.** 2-chamber T1 maps throughout the constant infusion at day 7 show the influx of tracer into the IOT (blue arrows) and INOT (yellow arrows).

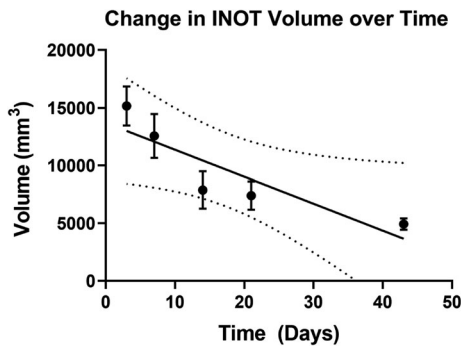


**Figure 4.** The INOT volume starts at its highest at day 3 and decreases over 42 days in all 8 animals.

GBCA must be being cleared similarly from the RT and blood.

The ECV in the INOT reached equilibrium between 50 and 60 minutes of onset for days 7 to 40 and likely did at the 60-minute time point for day 3 (see Figure 6), demonstrating that even with reduced blood flow in the INOT tissue, a 60-minute wash in was sufficient to obtain accurate values of ECV. However, the 60 min constant infusion in the IOT appears to not have reached equilibrium within the tissue, and hence, it is unlikely that the estimate of ECV is accurate. The data presented in Figures 4 and 6 at 7, 14, and 21 days suggest that ECV of IOT may actually be similar to that of INOT at the end of the 60 min infusion. However, in the early days following infarction, at day 3, the IOT-measured ECV was comparable to RT and much lower than the

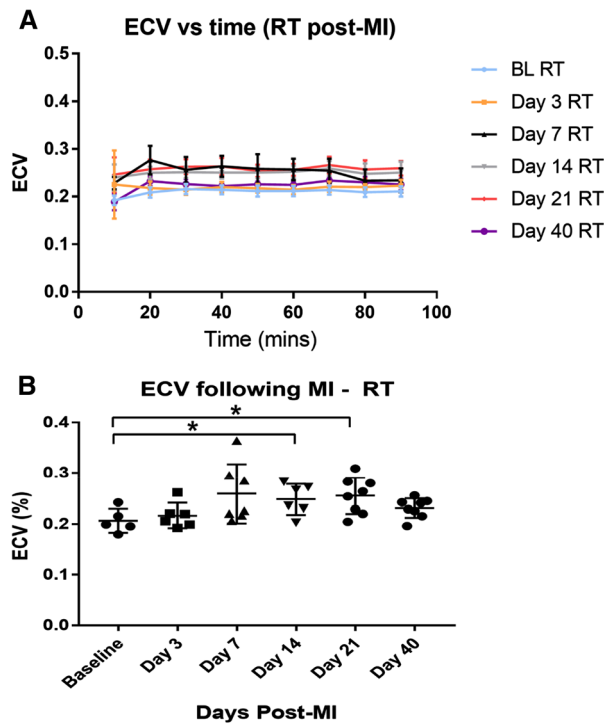


**Figure 5.** **A** ECV (mean  $\pm$  SEM) varies in the days following MI in the RT over the duration of the scan using the constant infusion protocol. **B** ECV values for each canine at each respective day post-MI in RT 60 min into the scan, at equilibrium, prior to washout of Gd-DTPA. \* represents a significant difference of ( $P < .05$ ).

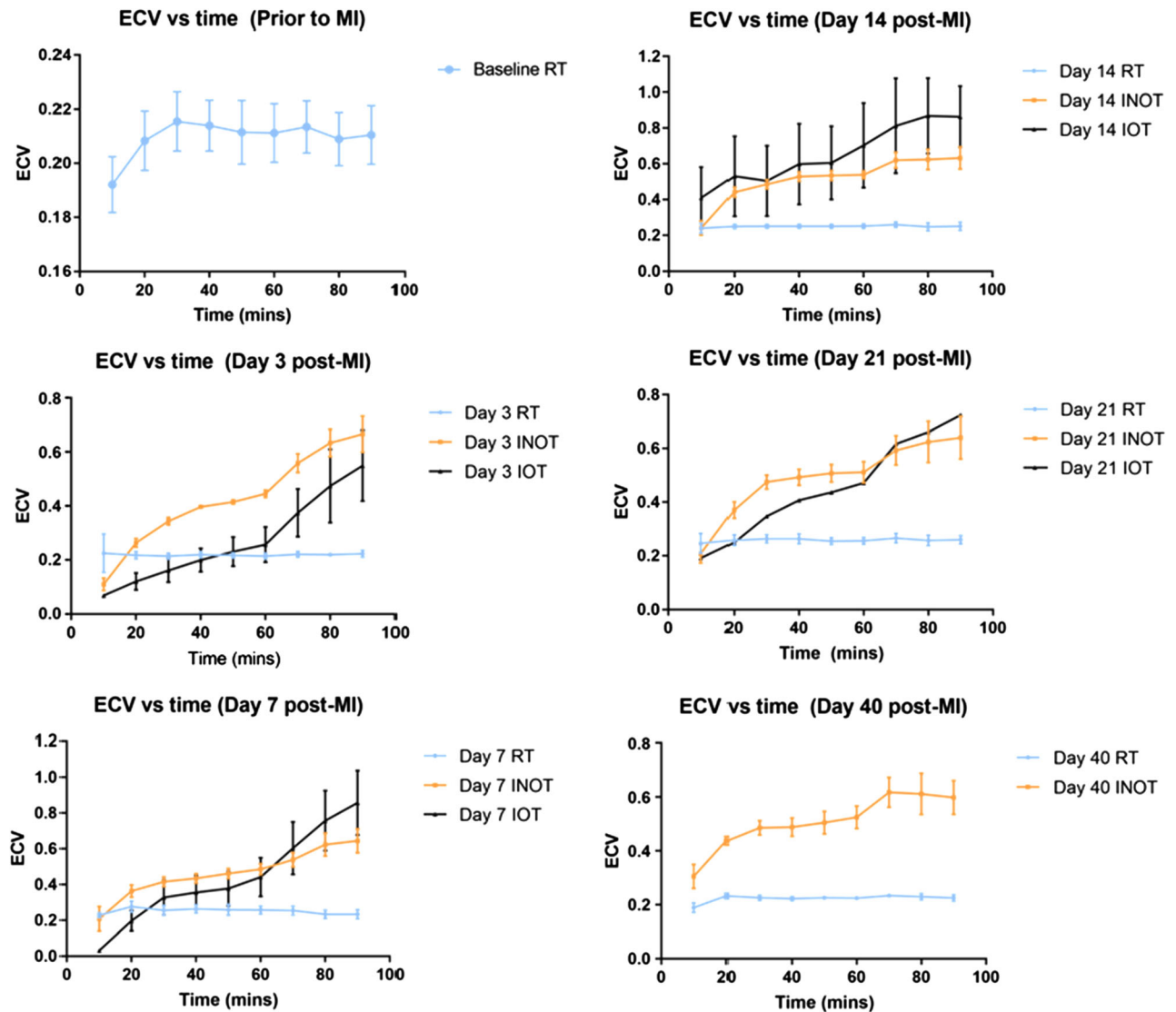


**Figure 6.** ECV measurements calculated in eight canine subjects measured every 10 minute for up to 90 minute after starting the constant infusion of Gd-DTPA. ECV was calculated in RT, INOT, and IOT at days 3, 7, 14, 21, and 40 post-MI and prior to MI. Data represented are mean  $\pm$  SEM. Constant infusion of Gd-DTPA was terminated at 60 minute followed by 30 minute of washout. Only one canine showed an IOT at day 21, and no IOT was seen for any canines 40 days post-MI. Figure 6 shows how the measured ECV varies with time for RT, IOT, and INOT. Clearly RT reaches equilibrium as quickly as seen in the normal myocardium measured at baseline with no change during washout. The measurement in the INOT reaches equilibrium well within the 60-minute constant infusion at all days except at day 3. The measurement in the IOT does not reach equilibrium except perhaps at day 7, though there was still a significant difference between the 50-minute and 60-minute time points. It is clear that the measurement of ECV is not accurate during washout for either INOT or IOT, independent of time, post-MI.

measured value in INOT. Nevertheless, compared to a bolus injection, significant penetration does occur with the 60 min constant infusion.<sup>11,16,25</sup>

Unlike RT, measurements of ECV during washout in the INOT and IOT should not be used as they were significantly elevated at all washout time points as

shown in Figures 6, 7, and S1. This is presumably because the blood flow is lower in the IOT and INOT and thus dramatically reduces Gd-DTPA clearance in the myocardium compared to blood, meaning that measured ECV appears artificially elevated.<sup>26</sup> This is the opposite to the beginning of the scan, where the ECV

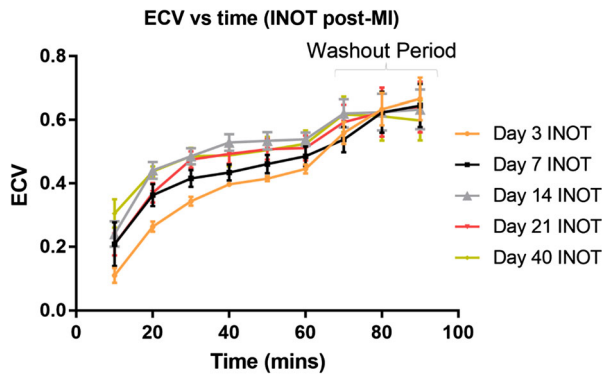


**Figure 7.** Shows ECV values for the INOT tissues for all canines post-infarction as a function of 60-minute constant infusion followed by 30 minute of washout. Measured ECV is increased during the washout period of Gd-DTPA.

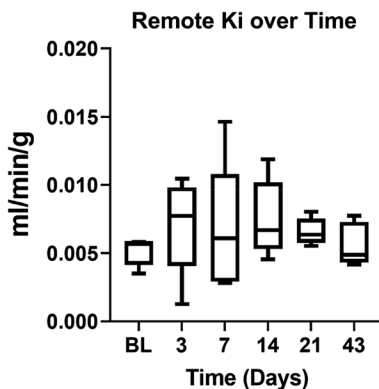


**Figure 8.** Remote Ki shows no significant difference over time though it appears as though there may be a rise over the first week. This plot shows the mean and interquartile ranges (box) and the maximum and minimum values (whiskers).

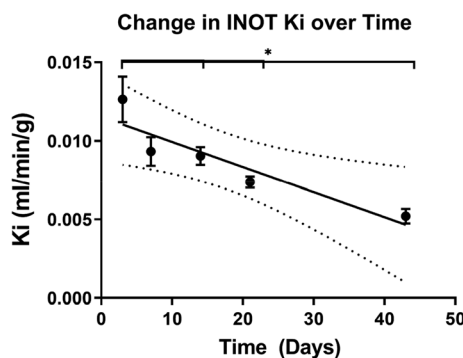


**Figure 9.** INOT Ki decreases linearly over time, returning to pre-infarct values ( $0.00514 \pm 0.00045$ ) at day 43. Ki in the INOT is significantly different from day 3 at day 14 ( $P = .0143$ ), day 21 ( $P = .0031$ ), and day 42 ( $P = .0003$ ).

is underestimated as the tracer entering the INOT lags behind Gd-DTPA concentrations in the blood. Note that these observations regarding achieving equilibrium in

RT, INOT, and IOT for GD-DTPA imply that FDG, which was concurrently injected with Gd-DTPA, would behave similarly.

Figure 10 shows that the functional assessments have a similar timeline for evolution of heart function as human patients post-MI with reduced ejection fraction.<sup>27</sup> There is a sharp decrease in ejection fraction at day 3 and recovery over the subsequent time points.

We found a significant increase in ECV in the RT at days 14 and 21 post-MI, but not at days 3 and 7. Increases in ECV in RT may reflect more generalized but less intense tissue edema and/or an early fibrotic response, not just limited to the area of acute ischemic injury, a pattern that has been shown in rats.<sup>8,28</sup> Cleutjens *et al.* have shown increased collagen protein deposition in rats in both infarcted and non-infarcted areas through upregulation of type 1 and type 3 collagen mRNA transcription.<sup>8</sup> This could potentially lead to the ECV increases that we observed post-MI.<sup>8,28</sup> At day 40, there was a  $p$  value of 0.06 for ECV in remote myocardium., A larger sample size could potentially have shown elevated ECV, 40 days post-MI. ECV calculation provides important, non-invasive insight into the pathophysiological mechanisms of cardiac remodeling post-MI and may serve as an important source of diagnostic, therapeutic, and prognostic decision making.<sup>10,29–31</sup> Specifically, the change in ECV in remote non-infarcted tissue provides strong evidence that there is a pathological process evolving in the early weeks post-infarct.<sup>8,28,32</sup> Future work is needed, such as validating this through measuring amount of fibrosis in histological tissue samples taken from RT and comparing it to tissue from sham-treated animals.

The decrease in the INOT volume using the 3D T1-weighted images (Figure 4) has underscored a long-standing debate. This decrease likely does not represent a degree of tissue repair but rather reflects permanently damaged myocardial tissue, in essence, shriveling over the days and weeks post-infarct. Note these data were taken while the blood and tissue concentrations were kept constant in the RT and to a large extent in the INOT tissue due to the constant infusion.

The FDG results that we observed were not as consistent as the ECV results. This is partially attributable to the lower spatial resolution of cardiac—FDG-PET in comparison to GBCA MRI, leading to potential partial volume issues in the discrimination of IOT from INOT. However, there should be a minimal partial volume effect from the left ventricular blood pool when assessing RT as myocardial edges were not included. As shown in Figure 8, there is a trend of an increase in Ki from baseline at days 3, 7, 14, and 21, though no significant changes were observed: day 3:  $P = .38$ ; day 7  $P = .32$ ; day 14:  $P = .11$ ; day 21:  $P = .19$ ; day



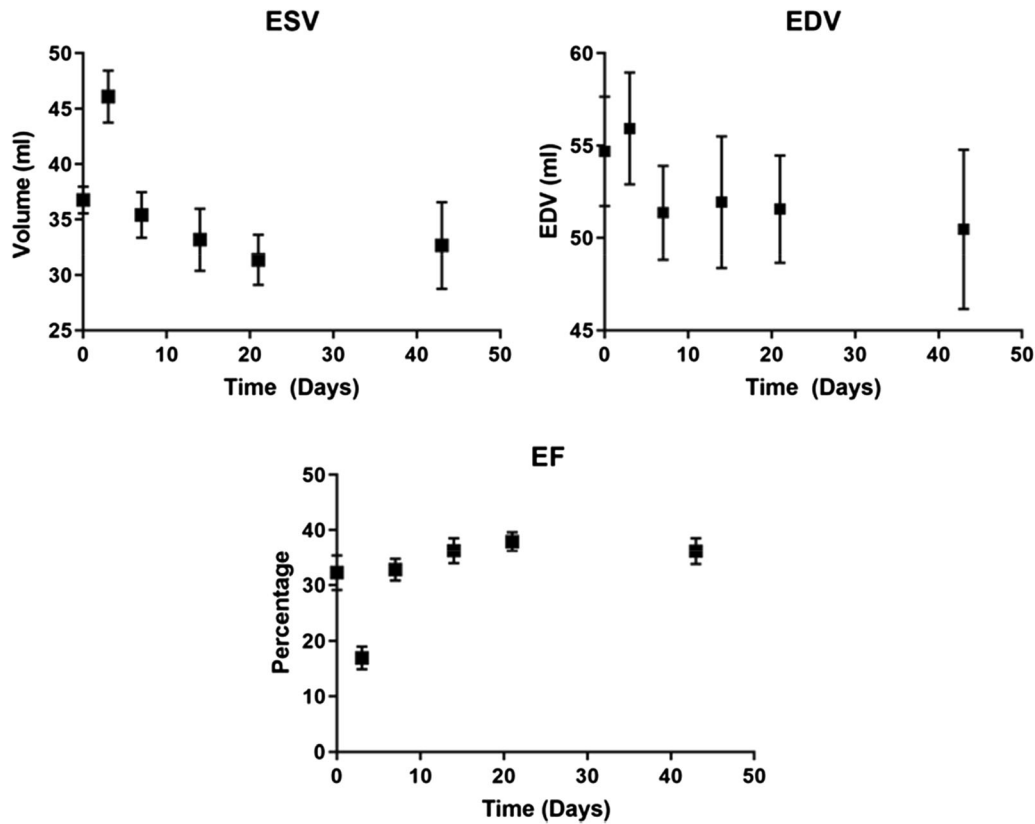


**Figure 10.** Ejection fraction over time: As in human patients, there is an initial drop in ejection fraction ( $P = .0013$ ) which then recovers in the following week and remains near baseline. This initial decline can be explained by an increased ESV ( $P = .0127$ ) with steady EDV.

43:  $P = .63$ . These values are also similar to what was found by Herrero et al in normal canine myocardium during suppression.<sup>33</sup> Figure 5B shows increases in ECV at days 7, 14, and potentially 43 days. Despite not large effects, this suggests that increases in ECV (potentially edema and fibrosis) are accompanied by cell-based inflammation in RT. Note how both results (Figures 5B and 8) suggest that by 43 days, both are proportionately reduced. If fibrosis had developed, it would seem unlikely that it would have resolved, suggesting that perhaps edema associated with the  $^{18}\text{F}$ -FDG-detected inflammation may have started to resolve.

Glucose metabolism in INOT decreased with time as shown in Figure 9, with Ki highest at 3 days (0.0125 mL/min/g) decreasing to approximately normal tissue values by day 43. In contrast, the Patlak analysis for INOT (see Figure S2) showed a significant increase in the extravascular exchangeable volume. This decrease in glucose metabolism in the INOT suggests that the number of metabolically active macrophages is decreasing or is being converted into M2-like macrophages,

which take up less FDG than M1-like macrophages.<sup>26</sup> It appears that the INOT experiences the highest level of inflammation within the first week following which it declines and returns to baseline by day 43. The IOT glucose metabolism was also significantly increased for the first week but could not be evaluated as a separate region distinct from the surrounding INOT after that due to the decreasing number of animals with an IOT at the later time points as there is apparent recovery from the initial microvascular injury. This strengthens the notion that anti-inflammatory treatment not only would be most effective within the first two weeks, but it also shows that the IOT may be an important factor influencing the perseverance of inflammation, especially since glucose metabolism in that region is probably underestimated. As we have shown here, even after the 60 min constant infusion, Gd-DTPA concentration was still increasing. This would suggest a corresponding increase in FDG concentrations within the IOT and that the methodology used in the experiments reported here underestimated the true glucose metabolic rate in the IOT.

Limitations of this study include the small number of animals, but even more so, the small number of animals with an IOT that was sustained through the period of observation, although this pattern of resolution of the regions of microvascular obstruction is by itself noteworthy. Another limitation is that not all animals could be imaged at every time point. While most animals had an IOT at day 3 and day 7, they disappeared at day 14, for all but two animals. More animals would also let us study the RT in more detail, since there is an increase in ECV on days 14 and 21 which may correspond to an inflammatory response. We have also found that ECV may be affected by myocardial glucose uptake suppression, i.e., larger by 13% in healthy myocardium.<sup>13</sup> Since all of these animals were suppressed equally, the trends found should not be affected, but actual ECV values may be slightly lower.

### NEW KNOWLEDGE GAINED

We have found evidence of a pathological process involving inflammation in the early weeks post-myocardial infarction. Increased ECV in the remote tissue suggests a pathological process in the RT. This research shows that a 60-minute constant infusion can be used to evaluate ECV and inflammation in the RT and INOT longitudinally but cannot be used to estimate the ECV in the IOT as the measured value does not reach equilibrium during the 60 minute.

### CONCLUSION

Here, we have shown rigorous longitudinal measurements of inflammation and ECV, measured during a combined infusion of FDG and GBCA. ECV in remote myocardium at 14- and 21-day post-MI was significantly greater than at baseline. The change in ECV in remote non-infarcted tissue provides strong evidence that there is a pathological process evolving in the early weeks post-infarct. As the concentration of FDG in the IOT continues to rise by the end of the constant infusion, it stands to reason that a bolus injection of FDG would underestimate the glucose metabolism in the IOT.

### Acknowledgements

*Wilk, B. is supported by an Ontario Graduate scholarship and a Lawson Internal Research Fund. This work was supported in part by Ontario Research Fund RE7-021 and Canadian Foundation for Innovation no. 11358. The authors would like to thank Siemens Health Care Limited for the in-kind contribution of the Myomaps software license. Both first authors contributed equally to this work.*

### Disclosure

*B. Wilk, H. Smailovic, G. Wisenberg, J. Sykes, J. Butler, M. Kovacs, J. D. Thiessen, and F. S. Prato have no conflicts of interest to disclose.*

### References

1. Braunwald E. Research advances in heart failure: A compendium. *Circ Res* 2013;113:633-45. <https://doi.org/10.1161/CIRCRESAHA.113.302254>.
2. Eitel I, Kubusch K, Strohm O, Desch S, Mikami Y, De Waha S, et al. Prognostic value and determinants of a hypointense infarct core in T2-weighted cardiac magnetic resonance in acute reperfused ST-elevation-myocardial infarction. *Circ Cardiovasc Imaging* 2011;4:354-62. <https://doi.org/10.1161/CIRCIMAGING.110.960500>.
3. Pfeffer MA, Braunwald E. Ventricular remodeling after myocardial infarction: Experimental observations and clinical implications. *Circulation* 1990;81:116-72. <https://doi.org/10.1161/01.CIR.81.4.1161>.
4. Ganame J, Messalli G, Dymarkowski S, Rademakers FE, Desmet W, Van De Werf F, et al. Impact of myocardial haemorrhage on left ventricular function and remodelling in patients with reperfused acute myocardial infarction. *Eur Heart J* 2009;30:1440-9. <https://doi.org/10.1093/eurheartj/ehp093>.
5. Kim RJ, Wu E, Rafael A, Chen EL, Parker MA, Simonetti O, et al. The use of contrast-enhanced magnetic resonance imaging to identify reversible myocardial dysfunction. *N Engl J Med* 2000. <https://doi.org/10.1056/NEJM200011163432003>.
6. Biesbroek PS, Amier RP, Teunissen PFA, Hofman MBM, Robbers LFHJ, van de Ven PM, et al. Changes in remote myocardial tissue after acute myocardial infarction and its relation to cardiac remodeling: A CMR T1 mapping study. *PLoS ONE* 2017. <https://doi.org/10.1371/journal.pone.0180115>.
7. Lurz JA, Luecke C, Lang D, Besler C, Rommel KP, Klingel K, et al. CMR-derived extracellular volume fraction as a marker for myocardial fibrosis: The importance of coexisting myocardial inflammation. *JACC Cardiovasc Imaging* 2018. <https://doi.org/10.1016/j.jcmg.2017.01.025>.
8. Cleutjens JPM, Verluyten MJA, Smits JFM, Daemen MJAP. Collagen remodeling after myocardial infarction in the rat heart. *Am J Pathol* 1995.
9. Radenkovic D, Weingärtner S, Ricketts L, Moon JC, Captur G. T1 mapping in cardiac MRI. *Heart Fail Rev* 2017. <https://doi.org/10.1007/s10741-017-9627-2>.
10. Thornhill RE, Prato FS, Wisenberg G, Moran GR, Sykes J. Determining the extent to which delayed-enhancement images reflect the partition-coefficient of Gd-DTPA in canine studies of reperfused and unperfused myocardial infarction. *Magn Reson Med* 2004. <https://doi.org/10.1002/mrm.20236>.
11. Salerno M, Janardhanan R, Jiji RS, Brooks J, Adenaw N, Mehta B, et al. Comparison of methods for determining the partition coefficient of gadolinium in the myocardium using T1 mapping. *J Magn Reson Imaging* 2013. <https://doi.org/10.1002/jmri.23875>.
12. Diesbourg LD, Prato FS, Wisenberg G, Drost DJ, Marshall TP, Carroll SE, et al. Quantification of myocardial blood flow and extracellular volumes using a bolus injection of Gd-DTPA: Kinetic modeling in canine ischemic disease. *Magn Reson Med* 1992;23:239-53. <https://doi.org/10.1002/mrm.1910230205>.
13. Smailovic H, Wilk B, Wisenberg G, Sykes J, Butler J, Hicks JW, et al. Simultaneous measurements of myocardial glucose

- metabolism and extracellular volumes with hybrid PET/MRI using concurrent injections of Gd-DTPA and [18F]FDG. *Submitted to J Nucl Cardiol* 2020.
14. Larson SR, Pieper JA, Hulten EA, Ficaro EP, Corbett JR, Murthy VL, et al. Characterization of a highly effective preparation for suppression of myocardial glucose utilization. *J Nucl Cardiol* 2019. <https://doi.org/10.1007/s12350-019-01786-w>.
  15. Merten CL, Knitelius HO, Assheuer J, Bergmann-Kurz B, Hedde JP, Bewermeyer H. MRI of acute cerebral infarcts: Increased contrast enhancement with continuous infusion of gadolinium. *Neuroradiology* 1999. <https://doi.org/10.1007/s002340050740>.
  16. Prato FS, Butler J, Sykes J, Keenlidside L, Blackwood KJ, Thompson RT, et al. Can the inflammatory response be evaluated using 18F-FDG within zones of microvascular obstruction after myocardial infarction? *J Nucl Med* 2015;56:299-304. <https://doi.org/10.2967/jnumed.114.147835>.
  17. Lau JMC, Laforest R, Sotoudeh H, Nie X, Sharma S, McConathy J, et al. Evaluation of attenuation correction in cardiac PET using PET/MR. *J Nucl Cardiol* 2017;24:839-46. <https://doi.org/10.1007/s12350-015-0197-1>.
  18. Patlak CS, Blasberg RG, Fenstermacher JD. Graphical evaluation of blood-to-brain transfer constants from multiple-time uptake data. *J Cereb Blood Flow Metab* 1983;3:1-7. <https://doi.org/10.1038/jcbfm.1985.87>.
  19. Lawrence J, Chang YMR, Szladovits B, Davison LJ, Garden OA. Breed-specific hematological phenotypes in the dog: A natural resource for the genetic dissection of hematological parameters in a mammalian species. *PLoS ONE* 2013. <https://doi.org/10.1371/journal.pone.0081288>.
  20. Higgins PJ, Garlick RL, Bunn HF. Glycosylated hemoglobin in human and animal red cells. Role of glucose permeability. *Diabetes* 1982. <https://doi.org/10.2337/diab.31.9.743>.
  21. Lortie M, Beanlands RSB, Yoshinaga K, Klein R, DaSilva JN, DeKemp RA. Quantification of myocardial blood flow with 82Rb dynamic PET imaging. *Eur J Nucl Med Mol Imaging* 2007;34:1765-74. <https://doi.org/10.1007/s00259-007-0478-2>.
  22. Anazodo U, Kewin M, Finger E, Thiessen J, Hadway J, Butler J, et al. Preliminary evaluation of MRI-derived input function for quantitative measurement of glucose metabolism in an integrated PET-MRI. *EJNMMI Phys* 2015;2:1-2. <https://doi.org/10.1186/2197-7364-2-s1-a80>.
  23. White SK, Sado DM, Fontana M, Banypersad SM, Maestrini V, Flett AS, et al. T1 mapping for myocardial extracellular volume measurement by CMR. *JACC Cardiovasc Imaging* 2013. <https://doi.org/10.1016/j.jcmg.2013.01.011>.
  24. Fedorov A, Beichel R, Kalpathy-Cramer J, Finet J, Fillion-Robin JC, Pujol S, et al. 3D Slicer as an image computing platform for the Quantitative Imaging Network. *Magn Reson Imaging* 2012. <https://doi.org/10.1016/j.mri.2012.05.001>.
  25. Bekkers SCAM, Yazdani SK, Virmani R, Waltenberger J. Microvascular obstruction. Underlying pathophysiology and clinical diagnosis. *J Am Coll Cardiol* 2010. <https://doi.org/10.1016/j.jacc.2009.12.037>.
  26. Borcherdt T, Beitar L, Langer LBN, Polyak A, Wester H-J, Ross TL, et al. Dissecting the target leukocyte subpopulations of clinically relevant inflammation radiopharmaceuticals. *J Nucl Cardiol* 2019.
  27. Chew DS, Heikki H, Schmidt G, Kavanagh KM, Dommasch M, Bloch Thomsen PE, et al. Change in left ventricular ejection fraction following first myocardial infarction and outcome. *JACC Clin Electrophysiol* 2018. <https://doi.org/10.1016/j.jacep.2017.12.015>.
  28. Sun Y, Cleutjens JPM, Diaz-Arias AA, Weber KT. Cardiac angiotensin converting enzyme and myocardial fibrosis in the rat. *Cardiovasc Res* 1994. <https://doi.org/10.1093/cvr/28.9.1423>.
  29. Kidambi A, Motwani M, Uddin A, Ripley DP, McDiarmid AK, Swoboda PP, et al. Myocardial extracellular volume estimation by CMR predicts functional recovery following acute MI. *JACC Cardiovasc Imaging* 2017. <https://doi.org/10.1016/j.jcmg.2016.06.015>.
  30. Thornhill RE, Prato FS, Wisenberg G, White JA, Nowell J, Sauer A. Feasibility of the single-bolus strategy for measuring the partition coefficient of Gd-DTPA in patients with myocardial infarction: Independence of image delay time and maturity of scar. *Magn Reson Med* 2006. <https://doi.org/10.1002/mrm.20830>.
  31. Haaf P, Garg P, Messroghli DR, Broadbent DA, Greenwood JP, Plein S. Cardiac T1 mapping and extracellular volume (ECV) in clinical practice: A comprehensive review. *J Cardiovasc Magn Reson* 2016. <https://doi.org/10.1186/s12968-016-0308-4>.
  32. Hinderer S, Schenke-Layland K. Cardiac fibrosis—A short review of causes and therapeutic strategies. *Adv Drug Deliv Rev* 2019. <https://doi.org/10.1016/j.addr.2019.05.011>.
  33. Herrero P. Quantification of myocardial glucose utilization by PET and 1-carbon-11-glucose. *J Nucl Cardiol* 2002;9:5-14. <https://doi.org/10.1067/mnc.2001.120635>.
- Publisher's Note** Springer Nature remains neutral with regard to jurisdictional claims in published maps and institutional affiliations.